PHILOSOPHICAL TRANSACTIONS OF THE ROYAL SOCIETY B

Phil. Trans. R. Soc. B (2005) **360**, 937–946
doi:10.1098/rstb.2005.1645
Published online 29 May 2005

Undirected graphs of frequency-dependent functional connectivity in whole brain networks

Raymond Salvador[1], John Suckling[1], Christian Schwarzbauer[2] and Ed Bullmore[1,*]

[1]*Brain Mapping Unit and Wolfson Brain Imaging Centre, Departments of Psychiatry and Clinical Neurosciences, Addenbrooke's Hospital, University of Cambridge, Cambridge CB2 2QQ, UK*
[2]*MRC Cognition and Brain Sciences Unit, 15 Chaucer Road, Cambridge CB2 2EF, UK*

We explored properties of whole brain networks based on multivariate spectral analysis of human functional magnetic resonance imaging (fMRI) time-series measured in 90 cortical and subcortical subregions in each of five healthy volunteers studied in the (no-task) resting state. We note that undirected graphs representing conditional independence between multivariate time-series can be more readily approached in the frequency domain than the time domain. Estimators of partial coherency and normalized partial mutual information ϕ, an integrated measure of partial coherence over an arbitrary frequency band, are applied. Using these tools, we replicate the prior observations that bilaterally homologous brain regions tend to be strongly connected and functional connectivity is generally greater at low frequencies [0.0004, 0.1518 Hz]. We also show that long-distance intrahemispheric connections between regions of prefrontal and parietal cortex were more salient at low frequencies than at frequencies greater than 0.3 Hz, whereas many local or short-distance connections, such as those comprising segregated dorsal and ventral paths in posterior cortex, were also represented in the graph of high-frequency connectivity. We conclude that the partial coherency spectrum between a pair of human brain regional fMRI time-series depends on the anatomical distance between regions: long-distance (greater than 7 cm) edges represent conditional dependence between bilaterally symmetric neocortical regions, and between regions of prefrontal and parietal association cortex in the same hemisphere, are predominantly subtended by low-frequency components.

Keywords: graph theory; Fourier domain; coherence; neuroimaging; network; multivariate time-series

1. INTRODUCTION

It is well known that neurophysiological time-series, measured by functional magnetic resonance imaging (fMRI), often demonstrate evidence of correlated activity between anatomically remote brain regions, even when the data have been acquired with a human subject lying quietly in the scanner 'at rest' (Biswal *et al.* 1995; Lowe *et al.* 1998; Greicius *et al.* 2002; Salvador *et al.* 2005). Resting state correlations have been discussed in terms of *functional connectivity*, broadly defined as the statistical association or dependency between anatomically distinct time-series (Aertsen *et al.* 1989; Friston *et al.* 1996; Horwitz 2003). In contrast to the related concept of effective connectivity, any measure of functional connectivity will be agnostic with respect to the direction of causal relations between brain regions that might subtend their observed dependency. Therefore, if regions A and B are functionally connected, then this tells us nothing about whether activity in A is driving B or vice versa. On this basis, we can see that a simple diagram of a brain network, in which a line is drawn between any pair of functionally connected regions, will constitute an undirected graph. This paper aims to rehearse the theory of undirected graphs based on multivariate time-series, and to illustrate how these theoretical tools can be applied in analysis of fMRI data. For a complementary application of directed graphs to analysis of effective connectivity in brain networks, see Eichler (2005).

We will show that a graph-theoretical analysis of brain connectivity in fMRI data is simplified if the metrics of association between regions are estimated in the frequency domain, for example, as coherencies or partial coherencies. This approach also accommodates a decomposition of functional connectivity between regions in terms of frequencies or frequency bands (Sun *et al.* 2004). In the electrophysiological literature, it has long been commonplace to estimate the coherence spectrum for a pair of electrodes, and often, it has been found that coherence is not equal at all frequencies, or that different systems of brain regions may be most coherent at different frequencies. In fMRI studies to date, it has been repeatedly shown that resting state correlations are often subtended by low-frequency (less than 0.1 Hz) components of the data (Biswal *et al.* 1995; Lowe *et al.* 1998; Cordes *et al.* 2000). The other main objective of this

* Author for correspondence (etb23@cam.ac.uk).

One contribution of 21 to a Theme Issue 'Multimodal neuroimaging of brain connectivity'.

Table 1. Cortical and subcortical regions (45 in each cerebral hemisphere, 90 in total) as anatomically defined by a prior template image in standard stereotaxic space.
(The abbreviations listed are those used in this paper, which differ slightly from the original abbreviations by Tzourio-Mazoyer *et al.* (2002). All regions are bilaterally symmetric; left-hand and right-hand sided homologues are distinguished by the suffixes L and R, respectively.)

region	abbreviation	region	abbreviation
precentral gyrus	PreCG	lingual gyrus	LING
superior frontal gyrus, dorsolateral	SFGdor	superior occipital gyrus	SOG
superior frontal gyrus, orbital part	ORBsup	middle occipital gyrus	MOG
middle frontal gyrus	MFG	inferior occipital gyrus	IOG
middle frontal gyrus, orbital part	ORBmid	fusiform gyrus	FFG
inferior frontal gyrus, opercular part	IFGoperc	postcentral gyrus	PoCG
inferior frontal gyrus, triangular part	IFGtriang	superior parietal gyrus	SPG
inferior frontal gyrus, orbital part	ORBinf	inferior parietal, but not supramarginal and angular gyri	IPL
rolandic operculum	ROL		
supplementary motor area	SMA	supramarginal gyrus	SMG
olfactory cortex	OLF	angular gyrus	ANG
superior frontal gyrus, medial	SFGmed	precuneus	PCUN
superior frontal gyrus, medial orbital	ORBsupmed	paracentral lobule	PCL
gyrus rectus	REC	caudate nucleus	CAU
insula	INS	lenticular nucleus, putamen	PUT
anterior cingulate and paracingulate gyri	ACG	lenticular nucleus, pallidum	PAL
median cingulate and paracingulate gyri	DCG	thalamus	THA
posterior cingulate gyrus	PCG	Heschl's gyrus	HES
hippocampus	HIP	superior temporal gyrus	STG
parahippocampal gyrus	PHG	temporal pole: superior temporal gyrus	TPOsup
amygdala	AMYG	middle temporal gyrus	MTG
calcarine fissure and surrounding cortex	CAL	temporal pole: middle temporal gyrus	TPOmid
cuneus	CUN	inferior temporal gyrus	ITG

paper is therefore to explore the frequency dependence of resting state connectivity more comprehensively by analysis of whole brain graphs based on metrics of association estimated in the frequency domain.

2. MATERIAL AND METHODS

(a) *fMRI datasets: acquisition and pre-processing*

Five sets of T2*-weighted gradient echo echoplanar imaging (EPI) data depicting blood oxygenation level dependent (BOLD) contrast were acquired, one each from five healthy volunteers in a no-task, resting state, using a Bruker Medspec S300 scanner operating at 3.0T (Bruker Medical, Ettlingen, Germany) in the Wolfson Brain Imaging Centre, Cambridge, UK. Volunteers were scanned while lying quietly with eyes closed for 37 min and 44 s. In this period, we acquired 2058 volumes with the following parameters: number of slices, 21 (interleaved); slice thickness, 4 mm; interslice gap, 1 mm; matrix size, 64×64; flip angle, 90°; TR, 1.1 s; TE, 27.5 ms; inplane resolution, 3.125 mm. The first 10 volumes were discarded prior to analysis to allow for T1 saturation effects, leaving 2048 volumes available for analysis of resting-state connectivity in each subject.

The datasets were initially corrected for geometrical displacements resulting from estimated head movement, and coregistered with the Montreal Neurological Institute (MNI) EPI template image, using SPM2 software (http://www.fil.ion.ucl.ac.uk/spm). The data were not spatially smoothed prior to regional parcellation using the anatomically labelled template image previously validated by Tzourio-Mazoyer *et al.* (2002). This parcellation divides each cerebral hemisphere into 45 anatomical regions of interest (ROIs), which are listed in table 1 together with the abbreviations used to refer to them in this study. Regional mean time-series were estimated for each individual simply by averaging the fMRI time-series over all voxels in each of 90 regions over the whole brain. Each regional mean time-series was further corrected for effects of head movement by regression on the time-series of translations and rotations of the head estimated in the course of initial movement correction by image realignment. The residuals of these regressions constituted the set of regional mean time-series used for undirected graph analysis.

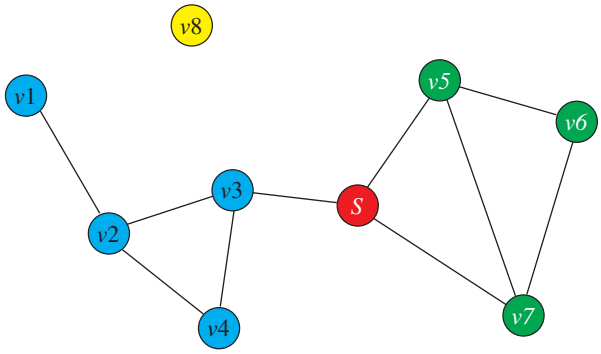

Figure 1. An undirected graph. Each edge between two vertices shows a relation of conditional dependence (these two vertices are dependent when conditioning on the rest of the vertices in the network). For instance, while $v1$ and $v2$ are still dependent when we condition on the rest of vertices, $v1$ and $v3$ are not (they are not linked by an edge). As a special case, one vertex may not be conditionally dependent on any other vertex, and will appear isolated in the graph (see $v8$). The properties of conditional independence can be extended to groups of variables. Thanks to the global Markov property, the set of blue vertices becomes independent from the set of green vertices when we fix S, the separator vertex. A separator may be formed by more than one vertex (here, $\{s, v3\}$ would also be a separator set).

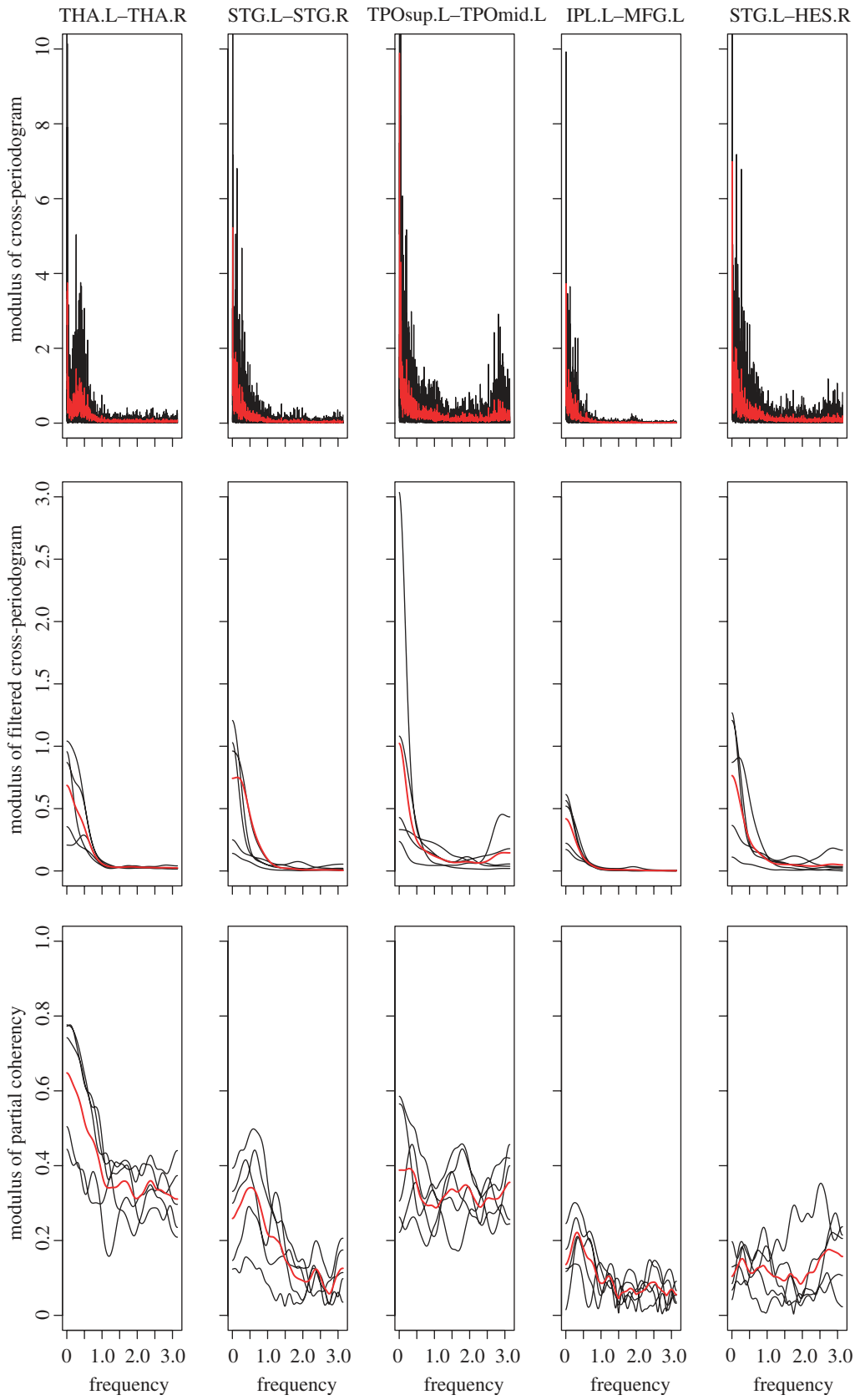

Figure 2. Spectral properties of functional connectivity between five pairs of brain regions in five subjects. The regional pairs include a short-distance, bilaterally symmetric pair (THA.L–THA.R); a long-distance, bilaterally symmetric pair (STG.L–STG.R); a short-distance, intrahemispheric pair (TPOsup.L–TPOmid.L); a long-distance, intrahemispheric pair (IPL.L–MFG.L); and a long-distance, bilaterally asymmetric pair (STG.L–HES.R). Top row shows the modulus of the cross-periodogram, individually estimated (black) and averaged over all subjects (red). Middle row shows the modulus of the filtered cross-periodogram, individually estimated (black) and averaged over all subjects (red). Bottom row shows the modulus of the partial coherencies (partial coherency spectra), individually estimated (black) and averaged over all subjects (red). Note the variability in partial coherency spectra between regional pairs, with a relatively stronger role of low frequencies in two of the long-range connections.

(b) *Undirected graph theory*

Graph theory has proved very useful in statistics to describe the dependence relations between random variables (Lauritzen 1996; Pearl 2000). At its core, lies the concept of a graph; a mathematical object defined by a pair $G=(V,E)$ in which V is a finite set of vertices (or nodes), and E is a set of edges connecting pairs of vertices in V (see figure 1).

Depending on the nature of the graph, these edges will describe different types of dependency between nodes. Thus, the category of graphs defined as undirected does not account for the directionality of connections, and the order of the components on each edge may be ignored ($(a,b)\in E$ implies $(b,a)\in E$). This lack of directionality has made them useful to portray conditional independence among components of random vectors (Whittaker 1990).

Given a multivariate Gaussian random vector $X=(X_1,\ldots,X_m)$, its conditional independence properties can be described by a graph, in which each component of X is drawn as a vertex of $V=\{V_1,\ldots,V_m\}$, and the absence of an edge (i,j) between V_i and V_j means that variables X_i and X_j are independent given the remainder of the variables

$$p(X_i,X_j|X_{\{1,\ldots,m\}\setminus i,j})=p(X_i|X_{\{1,\ldots,m\}\setminus i,j})p(X_j|X_{\{1,\ldots,m\}\setminus i,j}). \tag{2.1}$$

Here $p(\,)$ stands for a density function, and the symbol \ after a set denotes the same set without the elements specified on the right side of the operator. Under normality, equation (2.1) is equivalent to

$$\mathrm{COV}\{X_i-\hat{X}_i(X_{\{1,\ldots,m\}\setminus i,j}),X_j-\hat{X}_j(X_{\{1,\ldots,m\}\setminus i,j})\}=0 \tag{2.2}$$

where $\hat{X}_i(X_{\{1,\ldots,m\}\setminus i,j})$ is the best linear predictor of X_i given $X_{\{1,\ldots,m\}\setminus i,j}$.

An alternative, but homologous, way of defining conditional independence under multivariate normality was proposed by Dempster (1972). This definition is based on the inverse of the covariance matrix of X

$$\mathrm{COV}(X_i,X_j|X_{\{1,\ldots,m\}\setminus i,j})=0\Leftrightarrow\{\mathrm{COV}(X)^{-1}\}_{i,j}=0 \tag{2.3}$$

and it has important practical implications.

We note that a graph portraying pairwise conditional independences is said to hold the *pairwise Markov property* (Speed & Kiiveri 1986; Cowell *et al.* 1999). Interestingly, it also holds the more general *global Markov property*, which accounts for the conditional independence of any two mutually exclusive subsets X_A, X_B of variables of X, given a third exclusive subset S

$$p(X_A,X_B|S)=p(X_A|S)p(X_B|S). \tag{2.4}$$

S is said to be a separator and it contains sufficient vertices to intercept any path from a variable in X_A to a variable in X_B (see figure 1 for illustration). In summary, an undirected graph will not only be informative about the conditional dependence relations between pairs of variables, but also among any possible subsets of them.

(c) *Undirected graphs and multivariate time-series*

While standard conditional independence graphs seem adequate to describe relations between variables in many experimental applications, they do not fit naturally in the fMRI setting. This is mainly a consequence of the fact that these models were originally intended for vectors of random variables, which would not properly account for the temporal dimension of fMRI datasets. Recently, however, the theory of conditional independence graphs has been extended to multivariate time-series (see Brillinger 1996; Dahlhaus 2000; Timmer *et al.* 2000; Bach & Jordan 2004, among others).

In this context, a multivariate Gaussian stationary time-series $Y(t)=(Y_1(t),\ldots,Y_m(t))$ with $t\in Z$ (a multivariate stochastic process) will have a conditional independence graph $G=(V,E)$, depicting each one of the individual time-series as a vertex ($V=\{V_1,\ldots,V_m\}$). However, the absence of an edge (i,j) between two vertices V_i and V_j, that is, the conditional independence of time-series Y_i and Y_j given the remainder of the time-series, will have a much more restrictive meaning

$$(i,j)\notin E\Rightarrow\mathrm{COV}\{\varepsilon_i(t),\varepsilon_j(t+u)\}=0\quad\forall\,u\in Z, \tag{2.5}$$

where $\varepsilon_i(t)=Y_i(t)-\hat{Y}_i(t)[Y\setminus Y_i,Y_j]$ and $\hat{Y}_i(t)[Y\setminus Y_i,Y_j]$ is the best linear predictor (the conditional expectation) of the component of Y_i at time t, given all the values (at all time points) of all stochastic processes in the set except Y_i and Y_j. Thus, the absence of an edge (i,j) will mean that the correlation between the residuals after subtracting the best linear predictors will be zero for all possible lags. The global Markov property has also been proved for undirected graphs of multivariate time-series (Dahlhaus 2000).

(d) *Conditional dependence in the frequency domain*

Although conditional independence between two time-series has been defined in the time domain, serious difficulties arise when looking for proper time-domain estimators of conditional dependence. Specifically, to obtain estimates of the covariances of equation (2.5), we first require estimates of the best linear predictors. However, under a broadly stationary normal model, such estimates cannot be directly obtained from the time-series. Fortunately, as we will see below, analogous concepts to those described above can be used to develop estimates of conditional dependence in the frequency domain without having to estimate the best linear predictor.

Provided that the cross-covariance function between any two time-series, Y_i and Y_j is summable,

$$\sum_{u=-\infty}^{\infty}|\mathrm{COV}\{Y_i(t+u),Y_j(t)\}|<\infty, \tag{2.6}$$

we can use the cross-spectral density to define an analogous measure of conditional dependence in the frequency domain. The cross-spectral density between Y_i and Y_j at a given frequency λ is given by

$$f_{i,j}(\lambda)=\frac{1}{2\pi}\sum_{u=-\infty}^{\infty}\mathrm{COV}\{Y_i(t+u),Y_j(t)\}\exp(-\mathrm{i}\lambda u), \tag{2.7}$$

where $f_{i,j}(\lambda)$ is a complex 2π-periodic function, with $f_{i,j}(-\lambda)=f_{j,i}(\lambda)$ for real valued time-series, and is fully described by its values in the interval $[0,\pi]$. If we define $f(\lambda)$ as the square hermitian matrix containing the cross-spectral density values at frequency λ for all pairs of time-series, then we have a definition of conditional independence equivalent to equation (2.3) (Brillinger 1996; Bach & Jordan 2004). Thus,

$$\begin{aligned}&\mathrm{COV}\{\varepsilon_i(t),\varepsilon_j(t+u)\}=0\quad\forall\,u\in Z\Leftrightarrow\\&\{f(\lambda)^{-1}\}_{i,j}=0\quad\forall\,\lambda\in[0,\pi]\end{aligned} \tag{2.8}$$

This equivalence has important practical implications, because it avoids having to estimate the values of the best linear predictors directly.

Under the additional assumption of null expectations (which can be approximately justified by mean-subtracting the observed time-series), a first estimation of $f_{i,j}$ will be obtained from the discrete Fourier coefficients of y_i and y_j (the observed finite realizations of Y_i and Y_j), avoiding the estimation of their cross covariance function. Specifically,

if y_i is of length n, then its $k=0,\ldots,n-1$ discrete Fourier coefficients are given by

$$d_i(k) = \frac{1}{n}\sum_{t=0}^{n-1} y_i(t)\exp(-\mathrm{i}kt), \tag{2.9}$$

and the estimate of the values of the cross-spectral density (the cross-periodogram) for the n Fourier frequencies $\lambda_k = \lambda_k = 2\pi k/n$ will be $\hat{f}_{i,j}(\lambda_k) = d_i(k)\bar{d}_j(k)$, where the superscript bar denotes the complex conjugate.

The cross-periodogram is a very noisy estimate of the cross-spectral density (Brillinger 1981), and a linear filter is usually required to reduce its variance. Here, we applied the filter used by Bach & Jordan (2004)

$$W(q) = \frac{r\sqrt{2\pi}}{n}\mathrm{e}^{-\lambda_q^2 r^2/2}, \tag{2.10}$$

where $r \leq n^{-1/5}$ is a parameter that modulates the smoothness of the filter, leading to a more stable estimate of the spectral density

$$\hat{f}_{ij}(\lambda_k) = \sum_{q=-\infty}^{\infty} W(q)\left[d_i\bar{d}_j\right](\lambda_{k+q}) \tag{2.11}$$

Finally, the estimates of the inverses of $f(\lambda)$ for the different Fourier frequencies are obtained from $\hat{f}(\lambda)^{-1}$. However, owing to the finite character of the sampled time-series, we cannot expect that $\{\hat{f}(\lambda)^{-1}\}_{i,j}$ will be exactly zero when Y_i and Y_j are conditionally independent.

(e) *Quantifying the strength of connection in the frequency domain*

Confronting the situation opposite to equation (2.8), if $\{f(\lambda)^{-1}\}_{i,j} \neq 0$ for one or more frequencies, then Y_i and Y_j will be conditionally dependent, given the rest of the time-series, at these frequencies. Some measures of the strength of such conditional dependence have been developed. In the frequency domain, the partial coherency (different from the partial coherence defined in equation (2.13) below) is a standardized measure of strength specific for each possible λ, similar to the partial correlation coefficient in the time domain. However, unlike the partial correlation, the partial coherency is a complex quantity with bounded modulus: $|R(\lambda)_{i,j}| \in [0,1]$. Additional results defined in the next section will allow us to formulate the partial coherency in a way (see equation (2.22)) that makes its resemblance to a partial correlation more explicit.

In practical terms, the matrix of partial coherencies (for a given λ) is derived in an analogous way to the partial correlation matrix in a non-temporal setting (see Whittaker 1990). Specifically, the main step of the process involves the inversion of the spectral density matrix (the equivalent of the covariance matrix). If, following Dahlhaus (2000), we calculate

$$R(\lambda) = -\begin{pmatrix} [\{f(\lambda)^{-1}\}_{1,1}]^{-1/2} & & 0 \\ & \ddots & \\ 0 & & [\{f(\lambda)^{-1}\}_{m,m}]^{-1/2} \end{pmatrix} \times f(\lambda)^{-1} \begin{pmatrix} [\{f(\lambda)^{-1}\}_{1,1}]^{-1/2} & & 0 \\ & \ddots & \\ 0 & & [\{f(\lambda)^{-1}\}_{m,m}]^{-1/2} \end{pmatrix} \tag{2.12}$$

then the partial coherencies between any given pair of time-series Y_i and Y_j are given by the off-diagonal complex values of this matrix.

On the one hand, the modulus of $R(\lambda)_{i,j}$ will quantify the intensity of the link between both time-series at λ. This information is usually reported as the square of the modulus, known as partial coherence

$$\mathrm{PCoh}_{i,j}(\lambda) = |R(\lambda)_{i,j}|^2, \tag{2.13}$$

which is also restricted to the [0,1] interval (and it is analogous to the coefficient of determination in regression analysis). On the other hand, the argument of the complex number $R(\lambda)_{i,j}$ conveys information on the temporal synchronization of both signals (i.e. the averaged phase between the two coherent processes). Hence, two time-series may be strongly linked but with a delayed 'connection' time, or may be instantaneously connected, then having a zero argument.

Considering the high number of Fourier frequencies potentially involved in an analysis of partial coherences, it may be of interest to use summary parameters that integrate the information over the whole spectrum or frequency bands. Based on information theory, one such parameter is the partial mutual information. The partial mutual information can be defined in terms of partial coherences (Granger & Hatanaka 1964; Brillinger 1996)

$$\delta_{i,j} = -\frac{1}{2\pi}\int_{-\pi}^{\pi} \log\{1 - \mathrm{PCoh}_{i,j}(\lambda)\}\mathrm{d}\lambda \tag{2.14}$$

But this is unbounded, ranging from 0 when partial coherences are null in all frequencies to infinity when all are 1. However, a simple transformation may be applied to obtain a normalized partial mutual information (Granger & Lin 1994; Harvill & Ray 2000), with scores in the interval [0,1]

$$\phi_{i,j} = [1 - \exp\{-2\delta_{i,j}\}]^{1/2} \tag{2.15}$$

Estimates of $\delta_{i,j}$ and $\phi_{i,j}$ can be derived from observed time-series by substituting estimates of the partial coherences in equation (2.14), and by conducting a finite weighted sum over the Fourier frequencies instead of the definite integral. Alternatively, the sum can be restricted to a specific interval of frequencies, providing a normalized mutual information measure for that range of frequencies.

(f) *Estimating synchronicity of connections*

Although, as mentioned above, the argument of coherencies is related to the averaged phase, a simpler way to assess this issue is achieved in the time domain. Here, we apply some of the concepts and formulae given by Eichler *et al.* (2003) for spatial point processes.

The definition of the residuals of the best linear predictor presented in equation (2.5) leads naturally to the following definition of the partial cross-spectral density:

$$f^p_{i,j}(\lambda) = \frac{1}{2\pi}\sum_{u=-\infty}^{\infty} \mathrm{COV}\{\varepsilon_i(t), \varepsilon_j(t+u)\}\exp(-\mathrm{i}\lambda u) \tag{2.16}$$

Indeed, this expression is analogous to that of the cross-spectral density (see equation (2.7)), although it involves the residuals instead of the original values. $f^p_{i,j}(\lambda)$ is easily derived from the matrix $f(\lambda)^{-1}$, as can be deduced from Dahlhaus (2000) and the inverse variance lemma of Whittaker (1990)

$$f^p_{i,j}(\lambda) = \frac{-\{f(\lambda)^{-1}\}_{i,j}}{\{f(\lambda)^{-1}\}_{i,i}\{f(\lambda)^{-1}\}_{j,j} - |\{f(\lambda)^{-1}\}_{i,j}|^2} \tag{2.17}$$

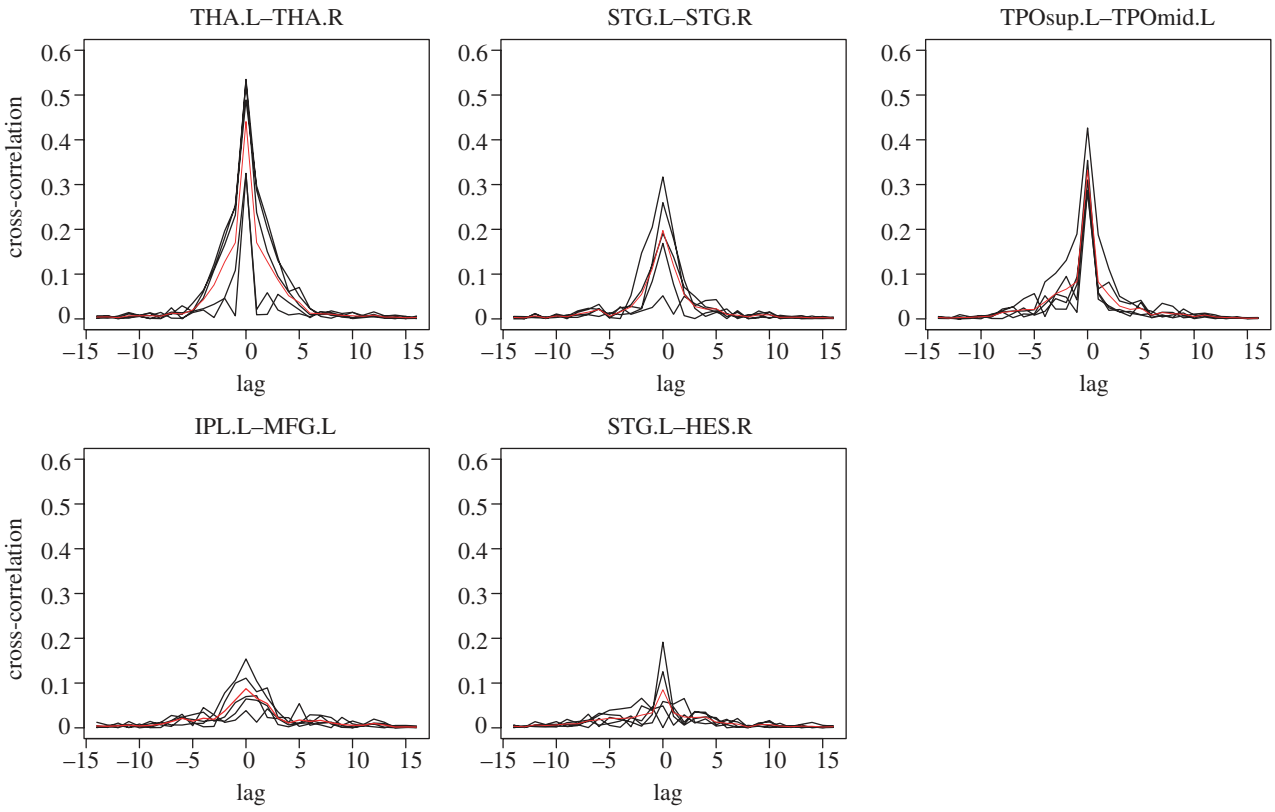

Figure 3. Partial cross-correlation functions for five pairs of brain regions in five subjects. The individual estimates for the five subjects are shown in black and their average is shown in red. For all regional pairs in all subjects, there is a clear peak at lag zero, and the group mean partial cross-correlation function is approximately symmetric.

(see Eichler *et al.* 2003 for an alternative formula). When $i=j$, a much simpler formula should be applied instead (Dahlhaus 2000); namely,

$$f^{p}_{i,i}(\lambda) = 1/\{f(\lambda)^{-1}\}_{i,i} \tag{2.18}$$

Here, it should be noted that $f^{p}_{i,j}(\lambda)$ is the cross-spectral density after conditioning on the rest of the variables ($\{1,\ldots,m\}\backslash i,j$), and, accordingly, equation (2.18) is conditioning on all variables except i ($\{1,\ldots,m\}\backslash i$). If we condition on both i and j, then a different formula should be used instead:

$$f_{i,i|\{1,\ldots,m\}\backslash i,j}(\lambda) = f^{p}_{i,i}(\lambda)/(1-\mathrm{PCoh}_{i,j}(\lambda)). \tag{2.19}$$

Next, by the Fourier inversion formula, we can go back to the cross-covariance functions of equation (2.16) linked to these cross-spectral densities. Specifically, for every possible lag u, this partial cross-covariance function will be given by

$$\mathrm{COV}^{p}_{i,j}(u) = \mathrm{COV}\{\varepsilon_i(t), \varepsilon_j(t+u)\} = \int_{-\pi}^{\pi} f^{p}_{i,j}(\lambda)\exp(\mathrm{i}\lambda u)\mathrm{d}\lambda. \tag{2.20}$$

Then, a standardized version of the partial cross-covariance function will given by the partial cross-correlation function

$$\rho^{p}_{i,j}(u) = \frac{\mathrm{COV}^{p}_{i,j}}{\sqrt{\mathrm{COV}_{i,i|\{1,\ldots,m\}\backslash i,j}(0)\mathrm{COV}_{j,j|\{1,\ldots,m\}\backslash i,j}(0)}}, \tag{2.21}$$

where $\mathrm{COV}_{i,i|\{1,\ldots,m\}\backslash i,j}(0)$ is the value at zero lag of the partial covariance function obtained by applying the same rationale of equation (2.20) to the conditional spectral density of equation (2.19).

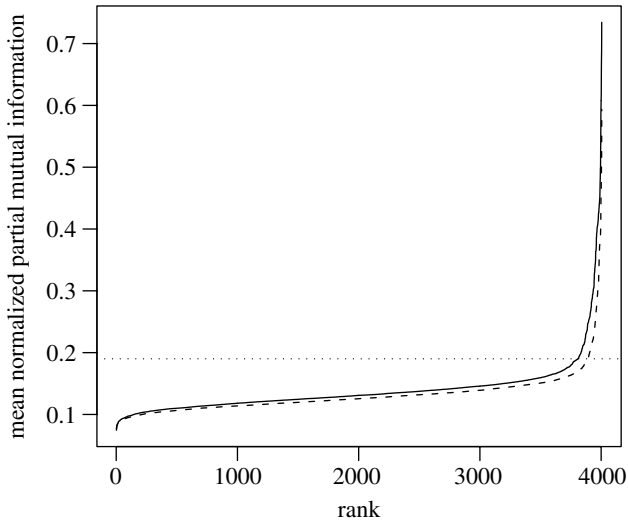

Figure 4. Sorted values of normalized partial mutual information ϕ estimated for all 4005 regional pairs and averaged over five subjects. Solid line shows the results for ϕ estimated in the low-frequency range and dashed line shows the results for ϕ estimated in the high-frequency range. It is clear that a small number of interregional connections are associated with unusually large values of ϕ in both frequency ranges. The horizontal dotted line indicates the heuristic threshold $\phi=0.19$ used to define conditional dependence between regions and so to prescribe an undirected edge between the corresponding vertices in a graph.

Next, estimates of the partial cross-covariance and cross-correlation functions can be derived from $\hat{f}(\lambda)^{-1}$ in the observed data. Substituting the values in equations (2.17), (2.18) and (2.19) will give the estimates of the partial

densities. Then, the discrete Fourier transform on the Fourier frequencies can be used instead of equation (2.20) to obtain the sample partial cross-covariances. When no specific model is given for the data, the estimates of the partial cross-covariance through the spectral densities overcome the problem of finding direct estimates from the residuals of the best linear predictor.

Finally, it should be noted that the introduction of the partial cross-spectral density in equation (2.16) allows an alternative definition of the partial coherency that (although being of no direct practical interest) clarifies its conceptual link to a partial correlation coefficient

$$R(\lambda)_{i,j} = \frac{f_{i,j|\{1,\ldots,m\}\setminus i,j}(\lambda)}{\sqrt{f_{i,i|\{1,\ldots,m\}\setminus i,j}(\lambda) f_{j,j|\{1,\ldots,m\}\setminus i,j}(\lambda)}}. \quad (2.22)$$

3. RESULTS

(a) *Cross-spectral densities, partial coherencies and partial cross-correlation functions estimated in functional MRI time-series*

We estimated the partial coherencies and partial cross-correlation functions for all 4005 possible inter-regional pairs, derived from 90 cortical and subcortical regions. However, for illustrative purposes, we will initially focus on the results for five pairs. The chosen pairs of functional MRI time-series are: (i) left and right thalamus (THA.L–THA.R)—a short-distance, bilaterally symmetric pair; (ii) left and right superior temporal gyrus (STG.L–STG.R)—a long-distance, bilaterally symmetric pair; (iii) left superior temporal pole and left-middle temporal pole (TPOsup.L–TPOmid.L)—a short-distance, (left) intrahemispheric pair; (iv) left inferior parietal lobule and left middle frontal gyrus (IPL.L–MFG.L)—a long-distance, (left) intrahemispheric pair; and (v) left superior temporal gyrus and right Heschl's gyrus (STG.L–HES.R)—a long-distance, bilaterally asymmetric pair.

For all five pairs, the modulus of the cross-periodogram (before and after smoothing; figure 2) was greatest at low frequencies. While this pattern was usually still present in the modulus of partial coherencies, their values were more variable between pairs. Short-distance pairs, both bilaterally symmetric (THA.L–THA.R) and intrahemispheric (TPOsup.L–TPOmid.L), had greater partial coherencies at high frequencies than two of the long-distance pairs. Both bilaterally symmetric (STG.L–STG.R) and long-distance, intrahemispheric (IPL.L–MFG.L) connections had greater partial coherencies at low frequencies. The third bilaterally asymmetric pair (STG.L–HES.R) had a slight dominance of high over low frequencies.

The partial cross-correlation functions were symmetrically peaked at zero lag for all five pairs, providing little evidence for temporally asymmetric effects in these data (figure 3).

(b) *Undirected graphs based on partial coherency in high- and low-frequency bands for all brain regional pairs*

To summarize the information contained in the partial coherency spectrums, we calculated the normalized partial mutual information in two frequency bands; specifically we integrated equation (2.14) over [0.0004, 0.1518 Hz] for the low-frequency band and over [0.3032, 0.4545 Hz] for the high-frequency band. The normalized partial mutual information ϕ, for each regional pair in each frequency band, was averaged over all five subjects. The sorted mean values of ϕ, plotted separately for high- and low-frequency bands in figure 4, show that a minority of regional pairs demonstrated exceptionally strong partial coherence over low- and high-frequency bands.

We identified the value $\phi = 0.19$ as the point of maximum inflexion for the order statistics of mutual information, shown in figure 4, and used this as a threshold to define edges in an undirected graph of whole brain functional connectivity. If $\phi > 0.19$ we drew an edge between the pair of regions, whereas if $\phi < 0.19$ the regions were not connected by an edge. The resulting graphs, drawn separately for high- and low-frequency bands, are shown in figure 5.

There are more edges in the low-frequency graph (197) than in the high-frequency graph (113). The coronal view of the graphs highlights bilaterally symmetric edges and almost all (44/45) possible bilaterally symmetric edges are represented in the low-frequency graph. There are only 24 in the high-frequency graph and they tend to be relatively short-distance (involving medial temporal, orbitofrontal and subcortical regions). The sagittal view of the high-frequency graph highlights the predominance of short-distance intrahemispheric edges, which form segregated dorsal and ventral paths in posterior cortex. The same view of the low-frequency map demonstrates richer local connectivity but also more long-distance intrahemispheric and bilaterally asymmetric edges (16 edges between regions separated by a Euclidean distance greater than 7 cm) compared with the low-frequency graph (three edges between regions greater than 7 cm apart). Long-distance intrahemispheric edges in the low-frequency graph, as shown more clearly in figure 6, predominantly involve regions of prefrontal cortex and parietal association cortex (IFGtriang.L–IPL.L, SFGmed.L–ANG.L, SFGdor.L–ANG.L, MFG.L–PCUN.L, SFGdor.R–ANG.R).

We can also visualize the differential importance of high- and low-frequency components in subtending short- and long-distance connections by plotting the mean normalized partial mutual information between each pair of regions in the brain versus the Euclidean distance between regional centroids in Talairach space (figure 7; see also Salvador *et al.* 2005 for a comparable plot of partial correlations estimated in the time domain versus Euclidean distance between regional centroids). It is clear that functional connectivity between regions separated by long distances is considerably stronger in the low-frequency band than the high-frequency band.

4. DISCUSSION AND CONCLUSIONS

We have described methods for constructing undirected graphs to represent conditional dependence relations between all pairs of major cortical and subcortical human brain regions. We have argued that this approach is facilitated using frequency domain estimators of conditional independence and, in particular, we have described in detail estimation of the partial coherencies and of an integrated measure over an arbitrary

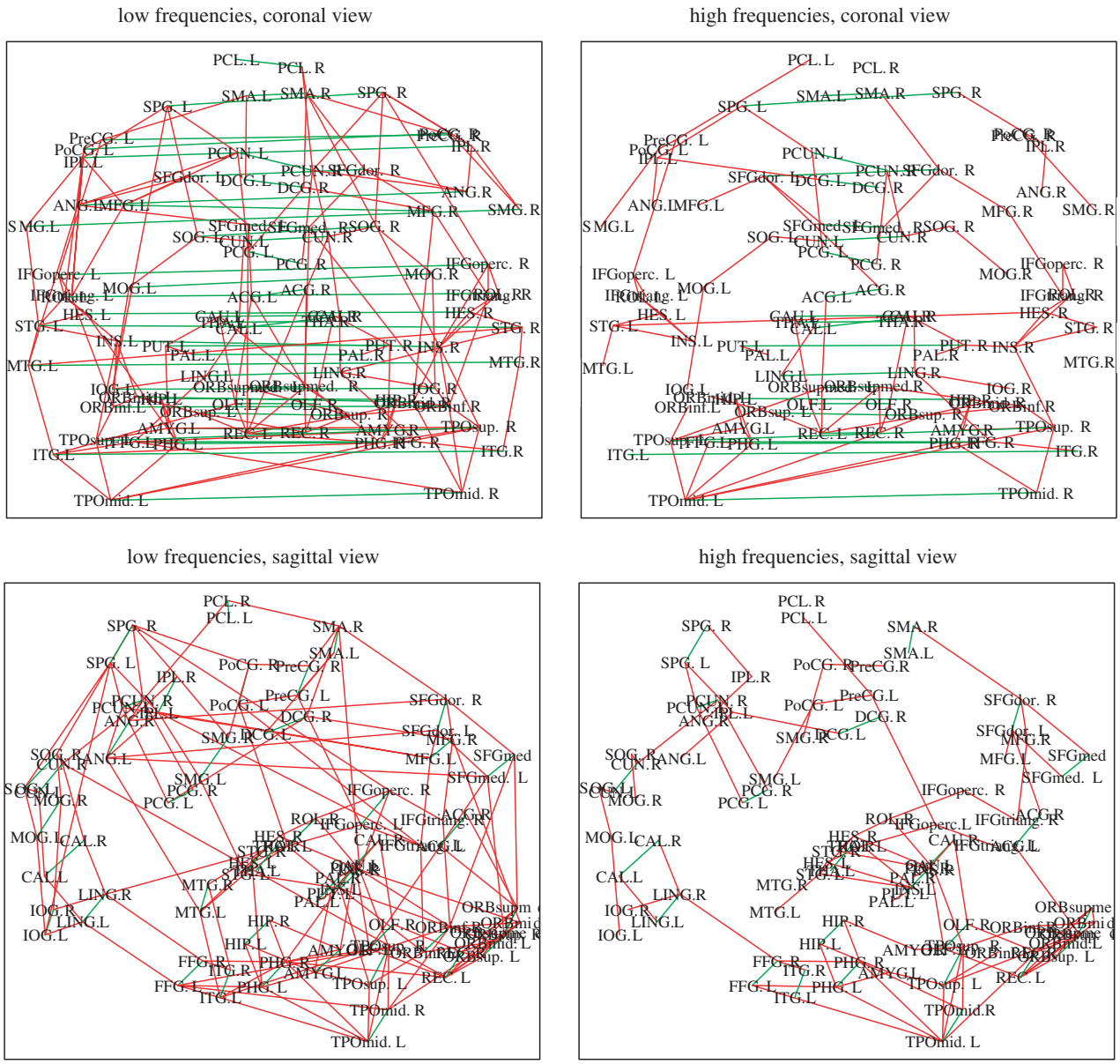

Figure 5. Undirected graphs of whole brain functional connectivity at low and high frequencies. Top row: coronal views of undirected graphs derived by thresholding normalized partial mutual information estimated for each of 4005 regional pairs in low (left) and high (right) frequency bands. Bilaterally symmetric edges are coloured green; other edges are coloured red. Regions are located by their centroid coordinates in the x and z dimensions of standard (Talairach) anatomical space; regional abbreviations are as listed in table 1. Bottom row: sagittal views of undirected graphs derived by thresholding normalized partial mutual information estimated for each of 4005 regional pairs in low (left) and high (right) frequency bands. Bilaterally symmetric edges are coloured green; other edges are coloured red. Regions are located by their centroid coordinates in the y and z dimensions of standard (Talairach) anatomical space.

frequency band, the normalized partial mutual information ϕ, as key measures of frequency-dependent functional connectivity between any pair of fMRI time-series. Using fMRI data acquired from five healthy volunteers in the resting (no-task) state, we have constructed whole brain graphs separately depicting salient conditional dependencies subtended by high- and low-frequency bands. To the best of our knowledge, these are the first maps to illustrate frequency dependence of entire human brain functional networks.

From a neurobiological perspective, several aspects of our results are consistent with prior analyses of resting state correlations estimated in the time domain (Biswal *et al.* 1995; Lowe *et al.* 1998; Salvador *et al.* 2005). For example, we have replicated previous observations that bilaterally homologous regions tend to be strongly and symmetrically connected, that low-frequency components generally subtend stronger functional connections than high-frequency components, and that local connectivity is generally stronger than long-distance connectivity. However, previous studies have often used low-pass filters prior to correlation analysis to focus exclusively on the low-frequency components of functional connectivity in a selected subset of regional pairs. The novelty of our results in this context is twofold. First, we have considered connectivity between all possible pairs of regions (defined by a previously parcellated template image). Secondly, we have mapped normalized partial mutual information for both high- and low-frequency bands. This has offered some preliminary insights into the variability of partial coherency spectra between

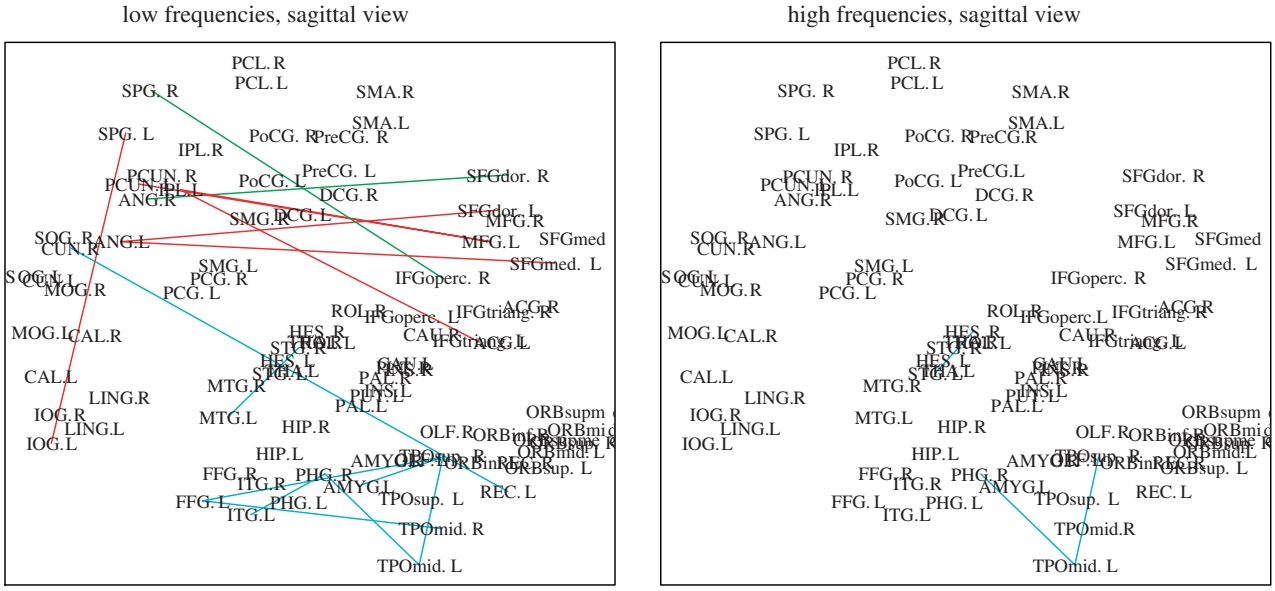

Figure 6. Long-distance edges in undirected graphs of whole brain functional connectivity at low and high frequencies. Sagittal views of low (left panel) and high (right panel) frequency graphs, illustrating only left (red) or right (green) intrahemispheric edges, or bilaterally asymmetric (blue) edges, between regions more than 7 cm apart. This display highlights the frequency dependence of long-distance intrahemispheric connections between regions of prefrontal and parietal association cortex.

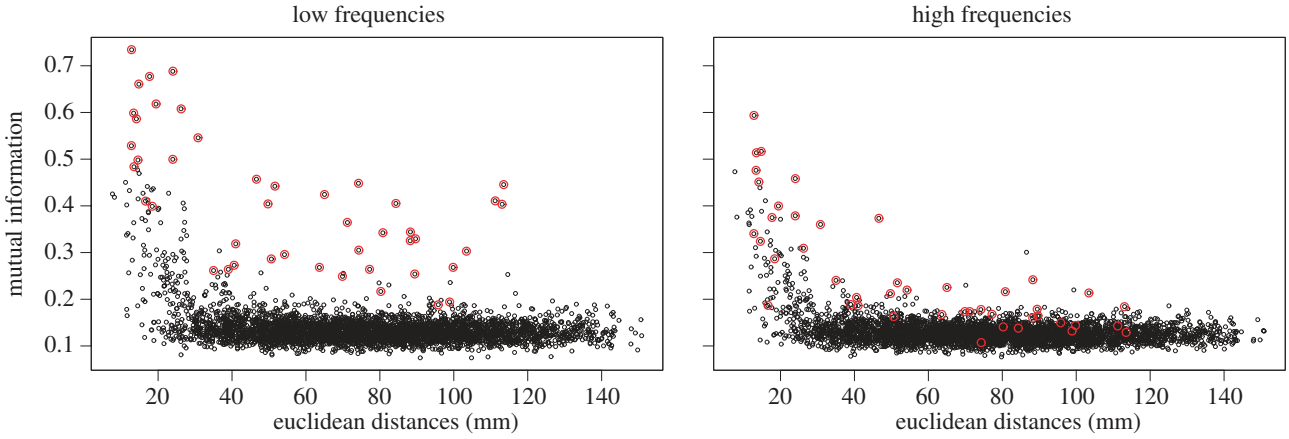

Figure 7. Dependency of functional connectivity on anatomical distance. Plots of Euclidean distances between centroids of each pair of regions (*x*-axis) versus their mean normalized partial mutual information (*y*-axis) in low- and high-frequency bands again demonstrates the importance of low-frequency components in subtending long-range connections, for example between bilaterally homologous regions (red dots).

different regional pairs. In particular, we have found that long-distance connections involving regions separated by a Euclidean distance greater than 7 cm are predominantly subtended by low-frequency components, whereas short-distance connections are also often subtended by high-frequency components. In short, it seems that low-frequency components may be differentially important in subtending long- and short-distance functional connectivity in the human brain.

It is beyond the scope of this paper to provide a comprehensive explanation for this difference in the partial coherency spectra of long- and short-distance functional connections. Long-distance functional connectivity, such as we have demonstrated between regions of prefrontal and parietal association cortex (Chafee & Goldman-Rakic 2000), or between bilaterally homologous regions of neocortex, is probably mediated by specialized white matter tracts. However, short-distance functional connectivity may be mediated by different anatomical substrates and confounded to a greater degree by nuisance sources of spatial covariance between time-series (including the point spread function of the scanner and effects of image normalization and interpolation). We note the analogous observations that between-electrode coherence of local field potentials, measured at multiple sites in visual cortex, falls off quickly as a function of both increasing distance and frequency (Leopold & Logothetis 2003). Nonetheless, (low-frequency) band-limited coherence does not decay as sharply as a function of distance between electrodes (Leopold *et al.* 2003). It will be interesting in future studies of resting state networks to apply novel methods for EEG/fMRI data fusion that can localize EEG rhythms, and may be able to elucidate the electrophysiological correlates of coherent, low-frequency fMRI oscillations (Martínez- Montes *et al.* 2004).

From a methodological perspective, we note that our method for thresholding the partial mutual

information to define an undirected edge between two regions is heuristic and does not quantify the probability of type I error in the resulting graphs. This reflects the lack of convenient parametric tests for the null hypothesis that group mean partial mutual information is zero. Future methodological work may include development of non-parametric tests, perhaps based on spatio-temporal wavelet resampling of resting fMRI time-series in different regions (Breakspear *et al.* 2004) to sample the null distribution of partial coherencies between regions. More fundamentally, it will be interesting to explore the complementary estimation of (partial) correlations between coefficients at different scales of the discrete wavelet transform as an alternative mathematical framework for analysis of the scaling properties of resting state functional connectivity (Salvador *et al.* 2005).

In summary, we have described methods for spectral analysis of multivariate time-series, and have shown for the first time how these can be used to construct frequency-dependent graphs of entire human brain functional networks. Our results provide preliminary evidence that there may be interesting differences in the partial coherency spectrum describing functional connectivity between different regional pairs, which appear to be related to the anatomical distance between them and may indicate distinct generative mechanisms for short- and long-distance resting state correlations in human fMRI data.

This neuroinformatics research was supported by a Human Brain Project grant from the National Institute of Biomedical Imaging and Bioengineering and the National Institute of Mental Health. The Wolfson Brain Imaging Centre is supported by an MRC Cooperative Group grant.

REFERENCES

Aertsen, A. M., Gerstein, G. L., Habib, M. K. & Palm, G. 1989 Dynamics of neuronal firing correlation: modulation of "effective connectivity". *J. Neurophysiol.* **61**, 900–917.

Bach, F. R. & Jordan, M. I. 2004 Learning graphical models for stationary time series. *IEEE Trans. Signal Processing* **52**, 2189–2199.

Biswal, B., Yetkin, F. Z., Haughton, V. M. & Hyde, J. S. 1995 Functional connectivity in the motor cortex of resting human brain using echoplanar MRI. *Magn. Reson. Med.* **34**, 537–541.

Breakspear, M., Brammer, M. J., Bullmore, E. T., Das, P. & Williams, L. M. 2004 Spatiotemporal wavelet resampling for functional neuroimaging data. *Hum. Brain Mapp.* **23**, 1–25.

Brillinger, D. R. 1981 *Time series. Data analysis and theory.* San Francisco: Holden Day.

Brillinger, D. R. 1996 Remarks concerning graphical models for the time series and point processes. *Rev. Econ.* **16**, 1–23.

Chafee, M. & Goldman-Rakic, P. S. 2000 Inactivation of parietal and prefrontal cortex reveals interdependence of neural activity during memory-guided saccades. *J. Neurophysiol.* **83**, 1550–1566.

Cordes, D., Haughton, V. M., Arfanakis, K., Carew, J. D., Turski, P. A., Moritz, C. H., Quigley, M. A. & Meyerand, M. E. 2000 Mapping functionally related regions of the brain with functional connectivity MR imaging. *Am. J. Neuroradiol.* **22**, 1326–1333.

Cowell, R. G., Dawid, A. P., Lauritzen, S. L. & Spiegelhalter, D. J. 1999 *Probabilistic networks and expert systems*. New York: Springer.

Dahlhaus, R. 2000 Graphical interaction models for multivariate time series. *Metrika* **51**, 157–172.

Dempster, A. P. 1972 Covariance selection. *Biometrics* **28**, 157–175.

Eichler, M., Dahlhaus, R. & Sandkühler, J. 2003 Partial correlation analysis for the identification of synaptic connections. *Biol. Cybern.* **89**, 289–302.

Eichler, M. 2005 A graphical approach for evaluating effective connectivity in neural systems. *Phil. Trans. R. Soc. B* **360**, 953–967. (doi:10.1098/rstb.2005.1641.)

Friston, K. J., Frith, C. D., Fletcher, P. C., Liddle, P. F. & Frackowiak, R. S. J. 1996 Functional topography: multidimensional scaling and functional connectivity in the brain. *Cereb. Cortex* **6**, 156–164.

Granger, C. W. G. & Hatanaka, M. 1964 *Spectral analysis of economical time series*. Princeton: Princeton Press.

Granger, C. & Lin, J. L. 1994 Using the mutual information coefficient to identify lags in nonlinear models. *J. Time Ser. Anal.* **15**, 371–384.

Greicius, M. D., Krasnow, B., Reiss, A. L. & Menon, V. 2002 Functional connectivity of the resting brain: a network analysis of the default mode hypothesis. *Proc. Natl Acad. Sci. USA* **100**, 253–258.

Harvill, J. & Ray, B. 2000 Lag identification for vector nonlinear time series. *Commun. Stat. Theory Methods* **29**, 1677–1702.

Horwitz, B. 2003 The elusive concept of brain connectivity. *NeuroImage* **19**, 466–470.

Lauritzen, S. L. 1996 *Graphical models*. Oxford: Clarendon Press.

Leopold, D. A. & Logothetis, N. K. 2003 Spatial patterns of local field activity in the monkey visual cortex. *Rev. Neurosci.* **14**, 195–205.

Leopold, D. A., Murayama, Y. & Logothetis, N. K. 2003 Very slow activity fluctuations in monkey visual cortex: implications for functional brain imaging. *Cereb. Cortex* **13**, 422–433.

Lowe, M. J., Mock, B. J. & Sorenson, J. A. 1998 Functional connectivity in single and multislice echoplanar imaging using resting state fluctuations. *NeuroImage* **7**, 119–132.

Martínez-Montes, E., Valdés-Sosa, P. A., Miwakeichi, F., Goldman, R. I. & Cohen, M. S. 2004 Concurrent EEG/fMRI analysis by multiway partial least squares. *NeuroImage* **22**, 1023–1034.

Pearl, J. 2000 *Causality. Models, reasoning and inference*. Cambridge: Cambridge University Press.

Salvador, R., Suckling, J., Coleman, M. R., Pickard, J. D., Menon, D. K. & Bullmore, E. 2005 Neurophysiological architecture of functional magnetic resonance images of human brain. *Cereb. Cortex* . Published online 5 January 2005. (doi:10.1093/cercor/bhi016.)

Speed, T. P. & Kiiveri, H. T. 1986 Gaussian Markov distributions over finite graphs. *Ann. Stat.* **14**, 138–150.

Sun, F. T., Miller, L. M. & D'Esposito, M. 2004 Measuring interregional functional connectivity using coherence and partial coherence analyses of fMRI data. *NeuroImage* **21**, 647–658.

Timmer, J. *et al.* 2000 Cross-spectral analysis of tremor time series. *Int. J. Bifurcat. Chaos* **10**, 2595–2610.

Tzourio-Mazoyer, N., Landeau, B., Papathanassiou, D., Crivello, F., Etard, O., Delcroix, N., Mazoyer, B. & Joliot, M. 2002 Automated anatomical labeling of activations in SPM using a macroscopic anatomical parcellation of the MNI MRI single-subject brain. *NeuroImage* **15**, 273–289.

Whittaker, J. 1990 *Graphical models in applied multivariate statistics*. Chichester: Wiley.